

1 HCPD-CA High-resolution climate projection dataset in Central

2 Asia ~~for ecological and hydrological applications~~

3 Yuan Qiu¹, Jinming Feng¹, Zhongwei Yan¹, and Jun Wang¹

4 1 Key Laboratory of Regional Climate-Environment for Temperate East Asia (RCE-TEA),

5 Institute of Atmospheric Physics, Chinese Academy of Sciences, Beijing 100029, China

6 Correspondence to: Jinming Feng, fengjm@tea.ac.cn

7 Abstract

8 Central Asia (referred to as CA) is one of the climate change Hot-Spots due to the fragile
9 ecosystems, ~~frequent natural hazards~~, strained water resources, and accelerated glacier
10 melting, which underscores the need of high-resolution climate projection datasets for
11 application to vulnerability, impacts, and adaption assessments ~~in ecological and hydrological~~
12 ~~systems in this region~~. In this study, a high-resolution (9km) climate projection dataset over
13 CA (the HCPD-CA dataset) is derived from dynamically downscaled results based on multiple
14 bias-corrected global climate models, and contains ~~four geostatic variables and~~ ten
15 meteorological elements that are widely used to drive ecological and hydrological models.
16 The reference and future periods are 1986-2005 and 2031-2050, respectively. The carbon
17 emission scenario is Representative Concentration Pathway (RCP) 4.5. The ~~results evaluation~~
18 shows ~~that~~ the data product has good quality in describing the climatology of all the elements
19 in CA ~~despite some systematic biases~~, which ensures the suitability of the dataset for future
20 research. ~~The m~~Main features of projected climate changes ~~in over~~ CA in the near-term future
21 ~~is are~~ strong warming (annual mean temperature increasing by 1.62-2.02°C) and significant
22 increase in downward shortwave and longwave flux at surface, with minor changes in other
23 elements (e.g., precipitation, relative humidity at 2m, and wind speed at 10m). The HCPD-
24 CA dataset presented here serves as a scientific basis for assessing the ~~potential~~ impacts of
25 ~~projected~~ climate changes over CA on many sectors, especially on ecological and
26 hydrological systems. It has the DOI <https://doi.org/10.11888/Meteoro.tpd.271759> (Qiu,
27 ~~is publicly available at~~ <http://data.tpdc.ac.cn/en/disallow/24e7467c-44a6-44ab-bbef-e6e346dd41d0/> (Qiu, 2021).

29 1. Introduction

30 Central Asia (referred to as CA, Fig. 1a) has complex terrain and diverse climates and is
31 among the most vulnerable regions to climate change due to fragile ecosystems (Zhang et al.,
32 2016; Seddon et al., 2016; Gessner et al., 2013), [frequent natural hazards](#) (Thurman,
33 2011; Burunciuc, 2020), [strained water resources](#) (Frenken, 2013), and accelerated glacier
34 melting (Narama et al., 2010; Sorg et al., 2012), which underscores the need to achieve high-
35 resolution climate projection datasets for application to vulnerability, impacts, and adaption
36 assessments [in ecological and hydrological systems](#). Global climate models (GCMs) can
37 describe the response of the global circulation to large-scale forcing, such as greenhouse gases
38 and solar radiation (Giorgi, 2019). But their horizontal resolutions are too coarse to account
39 for the effects of local-scale forcing and processes, such as complex topography, land cover
40 distribution, and dynamical processes occurring at the mesoscale (Giorgi et al., 2016; Qiu et
41 al., 2017; Torma et al., 2015). [Regional To obtain the accurate information on region-scale](#)
42 [climate change, dynamical downscaling has been developed and widely applied in regional](#)
43 [climate projections over many areas, like East Asia](#) (Zou and Zhou, 2016; Tang et al.,
44 2016; Jung et al., 2015; Jiang et al., 2021; Ji and Kang, 2013; Hong et al., 2017; Guo et al.,
45 2021; Bao et al., 2015; Zou and Zhou, 2017), [North America](#) (Wang and Kotamarthi,
46 2015; Racherla et al., 2012; Pierce et al., 2013; Giorgi et al., 1994; Di Luca et al., 2013,
47 2012; Wang et al., 2015), [and Europe](#) (Vautard et al., 2013; Jacob et al., 2014; Kotlarski et al.,
48 2014; Fischer et al., 2015; Kotlarski et al., 2015; Torma et al., 2015; Giorgi et al., 2016; Zittis et
49 al., 2019; Jacob et al., 2020; Déqué et al., 2007; Gao et al., 2006; Im et al., 2010). [climate models](#)
50 [\(RCMs\) have been applied to downscale the GCM outputs to finer scales](#) [Some efforts have](#)
51 [also been devoted on regional climate projection in CA with the dynamical downscaling](#)
52 [method](#) (Zhu et al., 2020; Ozturk et al., 2017; Mannig et al., 2013). However, their resolutions
53 are still low ($\geq 30\text{km}$), especially for the mountainous areas in the southeast. Moreover, most
54 of the previous RCM simulations [in CA](#) used a single GCM as the lateral boundary conditions,
55 which harbor high uncertainties in the projected climate changes.

56 The present authors carried out a study that involves the dynamical downscaling of
57 multiple bias-corrected GCMs for the CA region with an unprecedented horizontal resolution
58 of 9km. The future simulation period is set as 2031-2050 under Representative Concentration
59 Pathway (RCP) 4.5, with the reference period of 1986-2005. The simulated surface air

60 temperature and precipitation have been evaluated in a recent study (Qiu et al., 2021) and
61 meanwhile basic features of the projected climate changes have been demonstrated. The
62 results show that the high-resolution RCMs driven by bias-corrected GCMs are excellent in
63 simulating the local temperature and precipitation in CA and detect significant warming,
64 severer heatwaves, and drier conditions in this region in the near-term future.

65 To satisfy the urgent need of high-resolution climate data for assessing the potential
66 impacts of the projected climate changes on many sectors ecological and hydrological
67 applications in CA, especially on ecological and hydrological systems, the HCPD-CA (High-
68 resolution Climate Projection Dataset in CA) dataset is derived from the 9-km resolution
69 downscaled results, which includes four geostatic (time-invariant) variables and ten
70 meteorological elements (Table 1) that are widely used to drive ecological and hydrological
71 models. The geostatic variables are terrain height (HGT, m), land use category (LU_INDEX,
72 21 categories), land mask (LANDMASK, 1 for land and 0 for water), and soil category
73 (ISLTYP, 16 categories). The meteorological elements are daily precipitation (PREC,
74 mm/day), daily mean/maximum/minimum temperature at 2m (T2MEAN/T2MAX/T2MIN,
75 K), daily mean relative humidity at 2m (RH2MEAN, %), daily mean eastward and northward
76 wind at 10m (U10MEAN/V10MEAN, m/s), daily mean downward shortwave/longwave flux
77 at surface (SWD/LWD, W/m²), and daily mean surface pressure (PSFC, Pa). The present
78 paper is to introduce this dataset to the community. Sect. 2 describes the regional model and
79 experiments. Model evaluation and projected changes in the meteorological elements are in
80 Sect. 3. Added values of using 9-km resolution respect to using coarser resolutions are
81 discussed in Sect. 4 as well as uncertainties of the evaluation and the HCPD-CA dataset. Sect.
82 5 describes access to the data product and all codes and tools. Main results are concluded in
83 Sect. 6.

84 **2 Model and experiments**

85 **2.1 Regional model**

86 The Weather Research and Forecasting (WRF) model with version 3.8.1 (Skamarock et
87 al., 2008) is used to downscale the GCMs. It has two domains (Fig. 1b). The outer one covers
88 a large region, with a 27-km resolution and 290×205 grids. The inner one covers the CA
89 region, with a 9-km resolution and 409×295 grids. The model has 33 levels in the vertical

90 direction with its top fixed at 50 hPa. Its physical schemes are set based on our previous work
91 about the sensitivity study of different physical parameterizations of the WRF model in
92 simulating the local climate in CA (Wang et al., 2020).Details about them are in Qiu et al.
93 (2021).Spectral nudging with a weak coefficient of 3×10^{-5} is applied in the outer domain
94 (not in the inner one), which prevents possible model drift during the long-term integration
95 by relaxing the model simulations of wind, temperature, and moisture toward the driving
96 conditions. In addition to greenhouse gases and solar constant, the WRF model also considers
97 other external forcing, such as aerosols, volcanoes, and ozone, to make its inner external
98 forcing consistent with the driving GCMs.

99 The geogrid program in the WRF model is to define the simulation domains, and
100 interpolate various terrestrial datasets to the model grids (Wang et al., 2007). (Wang et al.,
101 2007)First, geogrid computes the latitude, longitude, and map scale factors at every grid point.
102 Then, it interpolates terrain height, land use category, soil category and other time-invariant
103 data to the model grides. Global datasets of each of these fields are provided through the WRF
104 download page
105 [\(https://www2.mmm.ucar.edu/wrf/users/download/get_sources_wps_geog.html\)](https://www2.mmm.ucar.edu/wrf/users/download/get_sources_wps_geog.html). The
106 HCPD-CA dataset contains four of the geostatic variables. In them, the terrain height (HGT)
107 data (Fig. S1) is from the United States Geological Survey (USGS) GTOPO30 elevation
108 dataset, the land use category (LU_INDEX) data (Table S1 and Fig. S2) is from the Moderate
109 Resolution Imaging Spectroradiometer (MODIS) 21 category land dataset, the soil category
110 (ISLTYP) data (Table S2 and Fig. S3) is from the global 5-minute United Nation FAO soil
111 category dataset, and the land mask (LANDMASK) data (Fig. S4) is calculated based on
112 LU_INDEX with the condition that the value of a grid cell is set as 1 (0) if land (water) area
113 at least accounts for 50%.

114 2.2 Bias-correction technique

115 MPI-ESM-MR (referred to as MPI, Table 2), CCSM4 (referred to as CCSM), and
116 HadGEM2-ES (referred to as Had) from Phase 5 of the Coupled Model Intercomparison
117 Project (CMIP5) are selected to drive the regional model. The reasons why we chose these
118 three GCMs are as below: they can provide all the variables that are needed to drive the
119 regional model; they have relatively high horizontal resolution (Table 2) among the CMIP5
120 models; they have fairly good performance in simulating the local temperature and

121 precipitation in CA (see Fig. S1 and S3 in Qiu et al., 2021), though systematic biases exist
122 partially due to their coarse resolutions. Since all GCMs suffer from some forms of bias (Done
123 et al., 2015; Ehret et al., 2012; Liang et al., 2008; Xu and Yang, 2012) that may propagate down
124 to the RCM outputs, the bias-correction technique developed by Bruyère et al. (2014) is
125 applied in this study to correct the climatology of the GCMs and allow synoptic and climate
126 variability to change.

127 Six-hourly GCM data in a 25-year base/future period (1981-2005/2026-2050), hereafter
128 referred to as GCM_{BP}/GCM_{FP} , are broken down into the 25-year mean 6-hourly annual cycle
129 over the base period (\overline{GCM}_{BP}) plus a 6-hourly perturbation term (GCM_{BP}'/GCM_{FP}'):

$$GCM_{BP} = \overline{GCM}_{BP} + GCM_{BP}' \quad (1)$$

$$GCM_{FP} = \overline{GCM}_{FP} + GCM_{FP}' \quad (2)$$

132 The ERA-Interim reanalysis data (Dee et al., 2011, Table 2) as “observations” (Obs) is
133 similarly broken down into the mean annual cycle (\overline{Obs}) and a perturbation term (Obs'):

$$Obs = \overline{Obs} + Obs' \quad (3)$$

135 The bias corrected GCM data for the base/future period, GCM_{BP}^*/GCM_{FP}^* , is then
136 constructed by replacing \overline{GCM}_{BP} from Eq. 1/2 with \overline{Obs} from Eq. 3:

$$GCM_{BP}^* = \overline{Obs} + GCM_{BP}' \quad (4)$$

$$GCM_{FP}^* = \overline{Obs} + GCM_{FP}' \quad (5)$$

139 Eq. 1-5 are applied to all the variables required to generate the initial and lateral boundary
140 conditions for the WRF model: zonal and meridional wind, geopotential height, air
141 temperature, relative humidity, sea surface temperature, mean sea level pressure, etc. In a
142 recent study (Qiu et al., 2021), we conducted the sensitivity experiments of using the bias-
143 correction technique, to quantify its contribution to improving the RCM simulation. The
144 results show that using the bias-correction technique largely reduced the biases in the
145 simulated annual and seasonal precipitation over CA respect to not using it and slightly
146 improved the model’s skill in simulating the spatial pattern of precipitation (see Fig. 4 in Qiu
147 et al., 2021).

148 The bias-corrected CCSM4 outputs (DOI: <https://doi.org/10.5065/D6DJ5CN4>) is
149 produced by Bruyère et al. (2014) with a 25-year base period (1981-2005) during the bias
150 correction. In this study, we produced the bias-corrected MPI-ESM-MR and HadGEM2-ES
151 outputs with the same base period as them. Note that the base period used during the bias

152 [correction is not necessary to be consistent with the reference period \(1986-2005\) of the RCM](#)
153 [simulations.](#)

154 **2.3 Experiments**

155 The RCM simulations with the bias-corrected GCMs (MPI, CCSM, and Had) as the
156 driving data are referred to as WRF_MPI_COR, WRF_CCSM_COR, and WRF_Had_COR,
157 respectively (“COR” means using the bias-correction technique). The reference-period
158 simulations are from December 1, 1985 to December 31, 2005 and the future runs are from
159 December 1, 2030 to the end of 2050 under a moderate carbon emission scenario RCP 4.5,
160 which is arguably the most policy-relevant scenario as the Nationally Determined
161 Contributions (NDCs) greenhouse gas emissions framework would produce similar
162 temperatures trajectories (Gabriel and Kimon, 2015). The first month in each simulation is
163 discarded as spin up. Fig. 2 shows the flow chart to produce the HCPD-CA dataset. [The](#)
164 [procedure can be divided into four steps. First, multiple-source observational data is used to](#)
165 [evaluate the WRF model with different combinations of physical schemes and then we found](#)
166 [the optimal combination of physical schemes for the WRF model. Second, the original GCMs](#)
167 [are bias corrected and the bias-corrected GCMs are used to drive the WRF model with the](#)
168 [optimal combination of physical schemes. Third, we conducted the dynamical downscaling](#)
169 [over CA and produced 9-km resolution downscaled results. At last, the HCPD-CA dataset](#)
170 [with certain variables and standard file formats is derived from the downscaled results.](#)

171 **3 Results**

172 **3.1 Model evaluation**

173 In Qiu et al. (2021), the key meteorological elements, surface air temperature and
174 precipitation [in the RCM simulations](#), have been evaluated with both gridded observations
175 and stations’ data (see Sect. 3.1 in the paper) and the results show good skills of the regional
176 model in simulating the local temperature and precipitation in CA during the reference period
177 (1986-2005). Accordingly, the ten meteorological elements (including surface air temperature
178 and precipitation) in the HCPD-CA dataset are evaluated here, to show the validity and
179 applicability of the dataset. Note that daily mean wind speed at 10m (referred to as
180 WS10MEAN) instead of U10MEAN and V10MEAN is evaluated.

181 Version 4 of the Climatic Research Units gridded Times Series (CRU TS v4, Harris et
182 al., 2020, Table 2) is applied to evaluate T2MEAN/T2MAX/T2MIN and the land component
183 of the fifth generation of European~~ECMWF (European Center for Medium Weather~~
184 ~~Forecasting)~~ atmospheric reanalysis (ERA5-Land, Hersbach et al., 2020, Table 2) land
185 monthly averaged data (referred to as ERA-Land) is used as “observations” to evaluate other
186 elements. Before the evaluation, the RCM outputs are interpolated to the grides of CRU TS
187 v4 (ERA5-Land) with the distance-weighted average (bilinear) method. We found that both
188 on the annual and seasonal scales, the interpolation methods conserved the area averaged
189 values in the model outputs with a bias of less than 1-2% between the original and new grids.
190 We thus concluded that our choice of interpolation procedure does not affect the main
191 conclusions of our work.

192 The high-resolution downscaled results (WRF_MPI_COR, WRF_CCSM_COR, and
193 WRF_Had_COR) are very close to the observational data in simulating the climatology of all
194 the elements in CA on the both annual and seasonal scales (Fig. 3-5, seasonal results not
195 shownhere). For instance, the spatial correlation coefficients (SCCs) of all the elements
196 annual mean values (except WS10MEAN) over CA are larger than 0.80. The SCCs of annual
197 mean WS10MEAN over CA are relatively small, in a range of 0.54-0.6064. The simulated
198 annual mean T2MEAN over the very north of Kazakhstan and the Pamirs has cold bias and
199 that over other areas generally has warm bias (Fig. 5Sa-c). However, the bias over most of
200 CA is within -2~2°C. The annual mean RH2MEAN is generally underestimated over CA
201 except some areas in the northern part and the Aral Sea (Fig. 6Sa-c). The regional model
202 overestimatedThe RCM simulations commonly overestimate the annual mean WS10MEAN
203 over the mountainous areas (Fig. 6Sd-f). Stronger annual mean SWD prevails in CA in each
204 simulation (Fig. 7Sa-c), with the mean errors (MEs) over the whole region in a range of
205 26.617.72-29.7731.43 W/m². Meanwhile, the regional model slightly underestimates annual
206 mean LWD (Fig. 7Sd-f). The bias in annual mean PSFC is very small over the majority of CA
207 (Fig. 7Sg-i). Table S3 summarizes the statistic metrics [SCCs, RMSEs, and mean errors (MEs)]
208 of all the annual mean variables over both CA and its climate subregions [northern CA (NCA),
209 middle CA (MCA), southern CA (SCA), and the mountainous areas (MT), see their scopes in
210 Fig. 1c], to help the readers easily check the quality of this data product in the areas they are
211 interested.

212 Fig. 6 shows mean annual cycle of the monthly values averaged over CA. It is seen that
213 the model outputs are generally close to the observations. The warm bias in T2MEAN mainly
214 occurs during May-August (Fig. 6a). The overestimation of SWD occurs throughout the year,
215 with the bias larger in the warm seasons than in the cold seasons (Fig. 6e). The results of
216 T2MAX and T2MIN are similar to those of T2MEAN (not shown here).

217 To sum up, the model-evaluation shows that the HCPD-CA dataset has good quality in
218 describing the climatology of all the ten-meteorological elements in CA despite some
219 systematic biases (e.g., stronger SWD), which ensures the suitability of the dataset for
220 ecological and hydrological applicationsassessment of future risk from climate change in CA.

221 3.2 Projected climate changes

222 Fig. 7 shows projected changes of the annual mean values in CA during 2031-2050,
223 relative to 1986-2005. All the RCM simulations exhibit significant warming over CA in the
224 near-term future, with the annual mean T2MEAN increasing by 1.62-2.02°C (Fig. 7a-c, range
225 depending on the simulation). Pronounced warming is found in the north, which is attributed
226 to the snow and surface albedo feedback (Qiu et al., 2021). Interestingly, enhanced warming
227 projected in many mountains in the world (Palazzi et al., 2019;Pepin et al., 2015;Rangwala et
228 al., 2013) is not found in CA (also see Fig. 7-8 in Qiu et al. (2021)). It poses a question if the
229 responses of ecological and hydrological systems to future warming in the Tien Shan and
230 Pamirs differ from those in other mountains, like Tibetan Plateau/Himalayas and Alps.

231 The annual mean precipitation (PREC) is projected to slightly increase by 0.01-0.02
232 mm/day (Fig. 7d-f). However, changes in few areas passed the significance test. The annual
233 mean RH2MEAN is projected simulated to slightly decrease by 0.68-1.28% (Fig. 7g-i), which
234 suggests a drier condition in CA in the coming decades and may affect the physical and
235 chemical properties of the local vegetations. Changes in wind speed (WS10MEAN) are
236 inconsistent among the RCM simulations (Fig. 7j-l). WRF_MPI_COR shows a slight increase
237 of 0.02m/s while others show a slight decrease, which highlights the uncertainties in the
238 projected changes. Downward shortwave/longwave flux (SWD/LWD) are projected to
239 significantly increase by 3.47-4.28 W/m² (Fig. 7m-o) and 7.13-9.61 W/m² (Fig. 7p-r),
240 respectively (Fig. 7m-r). Surface pressure (PSFC) is simulated to slightly increase by 0.15-
241 0.70 hPa in CA (Fig. 7s-u).

242 To sum up, the-main features of projected climate changes in CA in the near-term future

243 ~~is-are~~ strong warming and significant increases in downward shortwave and longwave flux,
244 with minor changes in other elements. Therefore, the HCPD-CA dataset provides
245 extraordinary warming scenarios for assessing the impacts of future warming on many sectors
246 (e.g., agriculture, the local ecological and hydrological systemss) in CA. Details about
247 changes in these meteorological elements (e.g., changes ~~at-on~~ the seasonal scale) are out of
248 the scope of the present paper and will be presented in further studies. Systematic analyses of
249 changes in surface air temperature, heatwaves and droughts are in Qiu et al. (2021).

250 **4 Discussion**

251 **4.1 Uncertainties in the evaluation**

252 To prove if considering the elevation differences between the observations and the model
253 grids during the evaluation will give a fairer assessment of the model's skills, we take
254 T2MEAN as an example and adjusted the simulated T2MEAN to the elevation of the
255 observations and then compared the adjusted T2MEAN with the observations. Here, we use
256 the records of T2MEAN on 58 stations across CA (see the stars in Fig. 1a) as observations,
257 which as well as the records of PREC on 52 stations (which is used in sect. 4.2, see the circles
258 in Fig. 1a) are from Global Historical Climatology Network (GHCN) of NOAA National
259 Climatic Data Center and have been quality controlled (Qiu et al., 2021). Note that a station
260 is compared with the model grid on which it is located. Fig. 8S shows the SCCs and RMSEs
261 of the simulated annual and seasonal T2MEAN over CA before and after adjusting. It is seen
262 that the simulated T2MEAN is more consistent with the observations after vertically
263 interpolating the model data to the elevation of the stations by the standard moist lapse rate
264 of 6.5 °C/km (Qiu et al., 2017). For instance, after adjusting the SCC of the annual T2MEAN
265 increases from 0.93 to 0.96 and its RMSE decreases from 2.52 to 2.25°C. This proves that the
266 regional model's skills may be underestimated if the elevation differences between the
267 observations and the model grids is not considered.

268 **4.2 9km vs 27km**

269 As discussed above, most of the previous RCM simulations in CA have horizontal
270 resolutions not higher than 30km. To show the added values of using 9-km resolution in this
271 study respect to using coarser resolutions, the evaluation metrics (SCC and RMSE) of the

272 simulated 9-km resolution precipitation in the inner domain of the WRF model are compared
273 with those of 27-km resolution precipitation in the outer domain (Fig. 8). As the gridded
274 observations (CRU TS v4, and ERA5-Land) have potential limitations in depicting the
275 climatology of [the elements precipitation](#) in CA, the metrics are calculated based on [58-the](#)
276 [aforementioned 52](#) stations' data across CA ([see red dots in Fig. 1a](#)), [which have been quality](#)
277 [controlled \(Qiu et al., 2021\). Note that a station is compared with the model grid on which it](#)
278 [is located.](#)

279 Compared with the 27-km resolution data, the 9-km resolution data largely increases
280 SCCs and reduces RMSEs, especially over the mountainous areas (see the [scope of](#) subregion
281 "MT" in Fig. 1c). For instance, over the mountainous areas, the ensemble-mean SCC of
282 annual precipitation increases from 0.38 to 0.58 (Fig. 8c) and the ensemble-mean RMSE of
283 annual precipitation decreases from 1.30 to 1.14 mm/day (Fig. 8d). This highlights the
284 necessity of improving the model resolution from $\geq 30\text{km}$ to 9km and the advantages of using
285 the HCPD-CA dataset for researches in CA.

286 **4.32 Uncertainties of the HCPD-CA dataset**

287 With the limitation of the computational and time cost, this study used three bias-
288 corrected GCMs from CMIP5 to do the dynamical downscaling over CA, which is an
289 improvement relative to using a single original GCM. However, it still harbors uncertainties
290 in the projected climate changes. As reported in the 1.5°C special report of the
291 Intergovernmental Panel on Climate Change (IPCC), we are on track to exceed 1.5°C warming
292 between 2030 and 2052 based on the current warming rate, and hence the near-term future
293 projection becomes more critical to human development than that for the end of this century.
294 Therefore, this study focuses on [projected](#) climate changes over CA in the near-term future
295 (2031-2050). Long-term continuous (e.g., 1986-2100) regional climate projections in CA are
296 more useful for studies in this region and will be conducted in the next stage. Land-use and
297 land-cover (LULC) in the WRF model [both in the historical and future simulations](#) is derived
298 from the [Moderate Resolution Imaging Spectroradiometer \(MODIS\)](#) data of 2002 (Wang et
299 al., 2007). Dramatic changes in [land-use and land-cover have happened in CA and are very](#)
300 [likely to be ongoing in the future](#) (Micklin, 2007; Ma et al., 2021; Chen et al., 2013; Li et al.,
301 2019), [such as water extent the shrinking](#) of the Aral Sea ([Micklin, 2007](#)) and [the expansion of](#)
302 [croplands and urbans](#). [The land-use and land-cover changes \(LULUCC\)](#) are not taken into

303 account during_in_the_our simulations, which brings uncertainties in simulating the local
304 historical climate in this area as well as projecting the climate changes in the future caused by
305 changes_in_LULC. A study about assessing the effects of the future LULCC on the local
306 climate in CA is in process and the model outputs from this study will be openly published as
307 a complement to the HCPD-CA dataset.

308 5. Data and code availability

309 The HCPD-CA dataset has the DOI <https://doi.org/10.11888/Meteoro.tpdc.271759> (Qiu,
310 2021) is available at <http://data.tpdc.ac.cn/en/disallow/24e7467e-44a6-44ab-bbef-e6e346dd41d0/> (Qiu, 2021). The files are stored in netCDF4 format and compiled using the
311 Climate and Forecast (CF) conventions. It contains four geostatic variables and ten
312 meteorological elements from three RCM simulations (WRF_CCSM_COR,
313 WRF_MPI_COR, and WRF_Had_COR) for a spatial domain covering the CA region (which
314 is consisted of Kazakhstan, Kyrgyzstan, Tajikistan, Turkmenistan, and Uzbekistan) and its
315 surrounding areas (see the domain “D02” in Fig. 1b). The dataset covers two continuous 20-
316 year periods, 1986-2005 and 2031-2050. Each year has 365 days (there is no leap year). We
317 provide smaller-size (monthly and annual) files as surrogates for larger-size (daily) files. The
318 names of the files containing the geostatic variables follow the order: [dataset name]_[variable
319 name].nc. For example, the file name, HCPD-CA_ISLTYP.nc, represents the soil category in
320 the HCPD-CA dataset. The names of the files containing the meteorological elements follow
321 the order: [dataset name]_[experiment name]_[element name]_[year].[time frequency].nc.
322 For example, the file name, HCPD-CA_WRF_CCSM_COR_T2MAX_2004.mon.nc,
323 represents the monthly mean T2MAX of 2004 from the experiment WRF_CCSM_COR in
324 the HCPD-CA dataset.

326 The WRF model is available at
327 https://www2.mmm.ucar.edu/wrf/users/download/get_source.html. The source code to do the
328 bias correction is available at <https://rda.ucar.edu/datasets/ds316.1/#!software>. The Climate
329 Data Operators (CDO, <https://code.mpimet.mpg.de/projects/cdo>), Python modules (like
330 netCDF4, Xarray, and Numpy), and NCAR Command Languages (NCL,
331 <https://www.ncl.ucar.edu/>) are recommended to do operations on the netCDF files.

332 **6. Conclusions**

333 A high-resolution (9km) projection climate dataset in CA (the HCPD-CA dataset),
334 containing four geostatic variables and ten meteorological elements, is derived from
335 dynamically downscaled results based on three bias-corrected GCMs (MPI-ESM-MR,
336 CCSM4, and HadGEM2-ES) from CMIP5 for ecological and hydrological applications to
337 vulnerability, impacts, and adaption assessments in this region. The reference and future
338 periods are 1986-2005 and 2031-2050, respectively. The carbon emission scenario is RCP4.5.
339 The model estimation evaluation shows good quality of the data product in describing the
340 climatology of all the meteorological elements in CA despite some systematic biases (e.g.,
341 stronger downward shortwave radiation throughout the year), which ensures the suitability of
342 the dataset. The RCM simulations commonly suggest strong warming over CA in the near-
343 term future, with the annual mean T2MEAN increasing by 1.62-2.02°C, and significant
344 increase in downward shortwave and longwave flux. Changes in other elements (e. g.,
345 precipitation, relative humidity at 2m, and wind speed at 10m) are minor. The HCPD-CA
346 dataset presented here serves as a scientific basis for assessing the impacts of climate change
347 over CA on many sectors, especially on ecological and hydrological systems.

348 **Author contribution**

349 All the authors made contributions to the conception or design of the work. YQ did the
350 analyses and drafted the work and others revised it.

351 **Competing interests**

352 The authors declare that they have no conflict of interest

353 **Acknowledgements**

354 This study was supported by the Strategic Priority Research Program of Chinese
355 Academy of Sciences (Grand No. XDA20020201) and the General Project of the National
356 Natural Science Foundation of China (Grand No. 41875134). The work was carried out at
357 National Supercomputer Center in Tianjin, and the calculations were performed on TianHe
358 +(A).this research was supported by TianHe Qingsuo Project – special fund project in the field
359 of climate, meteorology and ocean. The HCPD-CA dataset is provided by hosted at National

360 Tibetan Plateau Data Center (<http://data.tpdc.ac.cn>).

361 **References**

362 Bao, J., Feng, J., and Wang, Y.: Dynamical downscaling simulation and future projection of
363 precipitation over China, *Journal of Geophysical Research: Atmospheres*, 120, 8227-
364 8243, 2015.

365 Bruyère, C. L., Done, J. M., Holland, G. J., and Fredrick, S.: Bias corrections of global models
366 for regional climate simulations of high-impact weather, *Climate Dynamics*, 43, 1847-
367 1856, 10.1007/s00382-013-2011-6, 2014.

368 Burunciuc, L.: Natural disasters cost Central Asia \$10 billion a year – Are we doing enough
369 to prevent them?, *World Bank Blogs*, 2020.

370 Chen, X., Bai, J., Li, X., Luo, G., Li, J., and Li, B. L.: Changes in land use/land cover and
371 ecosystem services in Central Asia during 1990–2009, *Current Opinion in*
372 *Environmental Sustainability*, 5, 116-127, <https://doi.org/10.1016/j.cosust.2012.12.005>,
373 2013.

374 Dee, D. P., Uppala, S. M., Simmons, A., Berrisford, P., Poli, P., Kobayashi, S., Andrae, U.,
375 Balmaseda, M., Balsamo, G., and Bauer, d. P.: The ERA-Interim reanalysis:
376 Configuration and performance of the data assimilation system, *Quarterly Journal of the*
377 *royal meteorological society*, 137, 553-597, 2011.

378 Déqué, M., Rowell, D. P., Lüthi, D., Giorgi, F., Christensen, J. H., Rockel, B., Jacob, D.,
379 Kjellström, E., de Castro, M., and van den Hurk, B.: An intercomparison of regional
380 climate simulations for Europe: assessing uncertainties in model projections, *Climatic*
381 *Change*, 81, 53-70, 10.1007/s10584-006-9228-x, 2007.

382 Di Luca, A., de Elía, R., and Laprise, R.: Potential for added value in precipitation simulated
383 by high-resolution nested Regional Climate Models and observations, *Climate*
384 *Dynamics*, 38, 1229-1247, 10.1007/s00382-011-1068-3, 2012.

385 Di Luca, A., de Elía, R., and Laprise, R.: Potential for small scale added value of RCM's
386 downscaled climate change signal, *Climate Dynamics*, 40, 601-618, 10.1007/s00382-
387 012-1415-z, 2013.

388 Done, J. M., Holland, G. J., Brûyère, C. L., Leung, L. R., and Suzuki-Parker, A.: Modeling
389 high-impact weather and climate: lessons from a tropical cyclone perspective, *Climatic*
390 *Change*, 129, 381-395, 10.1007/s10584-013-0954-6, 2015.

391 Ehret, U., Zehe, E., Wulfmeyer, V., Warrach-Sagi, K., and Liebert, J.: HESS Opinions "Should
392 we apply bias correction to global and regional climate model data?", *Hydrol. Earth Syst.*
393 *Sci.*, 16, 3391-3404, 10.5194/hess-16-3391-2012, 2012.

394 Fischer, A. M., Keller, D. E., Liniger, M. A., Rajczak, J., Schär, C., and Appenzeller, C.:
395 Projected changes in precipitation intensity and frequency in Switzerland: a multi-model
396 perspective, *International Journal of Climatology*, 35, 3204-3219, 10.1002/joc.4162,
397 2015.

398 Frenken, K.: Irrigation in Central Asia in figures, *Food and Agriculture Organization of the*
399 *United Nations*, 2013.

400 Gabriel, K. A., and Kimon, K.: Analysis of scenarios integrating the INDCs, EUR - Scientific
401 and Technical Research Reports, 2015.

402 Gao, X., Pal, J. S., and Giorgi, F.: Projected changes in mean and extreme precipitation over
403 the Mediterranean region from a high resolution double nested RCM simulation,
404 *Geophysical Research Letters*, 33, 10.1029/2005GL024954, 2006.

405 Gessner, U., Naeimi, V., Klein, I., Kuenzer, C., Klein, D., and Dech, S.: The relationship
406 between precipitation anomalies and satellite-derived vegetation activity in Central Asia,
407 Global and Planetary Change, 110, 74-87,
408 <https://doi.org/10.1016/j.gloplacha.2012.09.007>, 2013.

409 Giorgi, F., Shields Brodeur, C., and Bates, G. T.: Regional Climate Change Scenarios over the
410 United States Produced with a Nested Regional Climate Model, *Journal of Climate*, 7,
411 375-399, 10.1175/1520-0442(1994)007<0375:RCCSOT>2.0.CO;2, 1994.

412 Giorgi, F., Torma, C., Coppola, E., Ban, N., Schär, C., and Somot, S.: Enhanced summer
413 convective rainfall at Alpine high elevations in response to climate warming, *Nature
414 Geoscience*, 9, 584-589, 10.1038/ngeo2761, 2016.

415 Giorgi, F.: Thirty Years of Regional Climate Modeling: Where Are We and Where Are We
416 Going next?, *Journal of Geophysical Research: Atmospheres*, 124, 5696-5723,
417 10.1029/2018jd030094, 2019.

418 Guo, D., Zhang, Y., Gao, X., Pepin, N., and Sun, J.: Evaluation and ensemble projection of
419 extreme high and low temperature events in China from four dynamical downscaling
420 simulations, *International Journal of Climatology*, 41, E1252-E1269, 2021.

421 Harris, I., Osborn, T. J., Jones, P., and Lister, D.: Version 4 of the CRU TS monthly high-
422 resolution gridded multivariate climate dataset, *Scientific Data*, 7, 109, 10.1038/s41597-
423 020-0453-3, 2020.

424 Hersbach, H., Bell, B., Berrisford, P., Hirahara, S., Horányi, A., Muñoz-Sabater, J., Nicolas,
425 J., Peubey, C., Radu, R., Schepers, D., Simmons, A., Soci, C., Abdalla, S., Abellan, X.,
426 Balsamo, G., Bechtold, P., Biavati, G., Bidlot, J., Bonavita, M., De Chiara, G., Dahlgren,
427 P., Dee, D., Diamantakis, M., Dragani, R., Flemming, J., Forbes, R., Fuentes, M., Geer,
428 A., Haimberger, L., Healy, S., Hogan, R. J., Hólm, E., Janisková, M., Keeley, S.,
429 Laloyaux, P., Lopez, P., Lupu, C., Radnoti, G., de Rosnay, P., Rozum, I., Vamborg, F.,
430 Villaume, S., and Thépaut, J.-N.: The ERA5 global reanalysis, *Quarterly Journal of the
431 Royal Meteorological Society*, 146, 1999-2049, <https://doi.org/10.1002/qj.3803>, 2020.

432 Hong, C., Zhang, Q., Zhang, Y., Tang, Y., Tong, D., and He, K.: Multi-year downscaling
433 application of two-way coupled WRF v3. 4 and CMAQ v5. 0.2 over east Asia for
434 regional climate and air quality modeling: model evaluation and aerosol direct effects,
435 *Geoscientific Model Development*, 10, 2447-2470, 2017.

436 Im, E. S., Coppola, E., Giorgi, F., and Bi, X.: Local effects of climate change over the Alpine
437 region: A study with a high resolution regional climate model with a surrogate climate
438 change scenario, *Geophysical Research Letters*, 37, 10.1029/2009GL041801, 2010.

439 Jacob, D., Petersen, J., Eggert, B., Alias, A., Christensen, O. B., Bouwer, L. M., Braun, A.,
440 Colette, A., Déqué, M., Georgievski, G., Georgopoulou, E., Gobiet, A., Menut, L.,
441 Nikulin, G., Haensler, A., Hempelmann, N., Jones, C., Keuler, K., Kovats, S., Kröner,
442 N., Kotlarski, S., Kriegsmann, A., Martin, E., van Meijgaard, E., Moseley, C., Pfeifer, S.,
443 Preuschmann, S., Radermacher, C., Radtke, K., Rechid, D., Rounsevell, M., Samuelsson,
444 P., Somot, S., Soussana, J.-F., Teichmann, C., Valentini, R., Vautard, R., Weber, B., and
445 Yiou, P.: EURO-CORDEX: new high-resolution climate change projections for
446 European impact research, *Regional Environmental Change*, 14, 563-578,
447 10.1007/s10113-013-0499-2, 2014.

448 Jacob, D., Teichmann, C., Sobolowski, S., Katragkou, E., Anders, I., Belda, M., Benestad, R.,
449 Boberg, F., Buonomo, E., Cardoso, R. M., Casanueva, A., Christensen, O. B.,
450 Christensen, J. H., Coppola, E., De Cruz, L., Davin, E. L., Dobler, A., Domínguez, M.,
451 Fealy, R., Fernandez, J., Gaertner, M. A., García-Díez, M., Giorgi, F., Gobiet, A.,

452 Goergen, K., Gómez-Navarro, J. J., Alemán, J. J. G., Gutiérrez, C., Gutiérrez, J. M.,
453 Gütter, I., Haensler, A., Halenka, T., Jerez, S., Jiménez-Guerrero, P., Jones, R. G., Keuler,
454 Kjellström, E., Knist, S., Kotlarski, S., Maraun, D., van Meijgaard, E., Mercogliano,
455 P., Montávez, J. P., Navarra, A., Nikulin, G., de Noblet-Ducoudré, N., Panitz, H.-J.,
456 Pfeifer, S., Piazza, M., Pichelli, E., Pietikäinen, J.-P., Prein, A. F., Preuschmann, S.,
457 Rechid, D., Rockel, B., Romera, R., Sánchez, E., Sieck, K., Soares, P. M. M., Somot, S.,
458 Srnec, L., Sørland, S. L., Termonia, P., Truhetz, H., Vautard, R., Warrach-Sagi, K., and
459 Wulfmeyer, V.: Regional climate downscaling over Europe: perspectives from the
460 EURO-CORDEX community, *Regional Environmental Change*, 20, 51,
461 10.1007/s10113-020-01606-9, 2020.

462 Ji, Z., and Kang, S.: Double-nested dynamical downscaling experiments over the Tibetan
463 Plateau and their projection of climate change under two RCP scenarios, *Journal of the*
464 *atmospheric sciences*, 70, 1278-1290, 2013.

465 Jiang, R., Sun, L., Sun, C., and Liang, X.-Z.: CWRF downscaling and understanding of China
466 precipitation projections, *Climate Dynamics*, 10.1007/s00382-021-05759-z, 2021.

467 Jung, C.-Y., Shin, H.-J., Jang, C. J., and Kim, H.-J.: Projected change in East Asian summer
468 monsoon by dynamic downscaling: Moisture budget analysis, *Asia-Pacific Journal of*
469 *Atmospheric Sciences*, 51, 77-89, 2015.

470 Kotlarski, S., Keuler, K., Christensen, O. B., Colette, A., Déqué, M., Gobiet, A., Goergen, K.,
471 Jacob, D., Lüthi, D., van Meijgaard, E., Nikulin, G., Schär, C., Teichmann, C., Vautard,
472 R., Warrach-Sagi, K., and Wulfmeyer, V.: Regional climate modeling on European scales:
473 a joint standard evaluation of the EURO-CORDEX RCM ensemble, *Geosci. Model Dev.*,
474 7, 1297-1333, 10.5194/gmd-7-1297-2014, 2014.

475 Kotlarski, S., Lüthi, D., and Schär, C.: The elevation dependency of 21st century European
476 climate change: an RCM ensemble perspective, *International Journal of Climatology*, 35,
477 3902-3920, 10.1002/joc.4254, 2015.

478 Liang, X.-Z., Kunkel, K. E., Meehl, G. A., Jones, R. G., and Wang, J. X. L.: Regional climate
479 models downscaling analysis of general circulation models present climate biases
480 propagation into future change projections, *Geophysical Research Letters*, 35,
481 <https://doi.org/10.1029/2007GL032849>, 2008.

482 Ma, X., Zhu, J., Yan, W., and Zhao, C.: Projections of desertification trends in Central Asia
483 under global warming scenarios, *Science of The Total Environment*, 781, 146777,
484 <https://doi.org/10.1016/j.scitotenv.2021.146777>, 2021.

485 Mannig, B., Müller, M., Starke, E., Merkenschlager, C., Mao, W., Zhi, X., Podzun, R., Jacob,
486 D., and Paeth, H.: Dynamical downscaling of climate change in Central Asia, *Global and*
487 *Planetary Change*, 110, 26-39, <https://doi.org/10.1016/j.gloplacha.2013.05.008>, 2013.

488 Micklin, P.: The Aral Sea disaster, in: *Annual Review of Earth and Planetary Sciences*, *Annual*
489 *Review of Earth and Planetary Sciences*, 47-72, 2007.

490 Narama, C., Kääb, A., Duishonakunov, M., and Abdurakhmatov, K.: Spatial variability of
491 recent glacier area changes in the Tien Shan Mountains, Central Asia, using Corona (~
492 1970), Landsat (~ 2000), and ALOS (~ 2007) satellite data, *Global Planet Change*, 71,
493 42-54, 2010.

494 Ozturk, T., Turp, M. T., Türkeş, M., and Kurnaz, M. L.: Projected changes in temperature and
495 precipitation climatology of Central Asia CORDEX Region 8 by using RegCM4.3.5,
496 *Atmospheric Research*, 183, 296-307, <https://doi.org/10.1016/j.atmosres.2016.09.008>,
497 2017.

498 Palazzi, E., Mortarini, L., Terzago, S., and von Hardenberg, J.: Elevation-dependent warming

499 in global climate model simulations at high spatial resolution, *Climate Dynamics*, 52,
500 2685-2702, 10.1007/s00382-018-4287-z, 2019.

501 Pepin, N., Bradley, R. S., Diaz, H. F., Baraer, M., Caceres, E. B., Forsythe, N., Fowler, H.,
502 Greenwood, G., Hashmi, M. Z., Liu, X. D., Miller, J. R., Ning, L., Ohmura, A., Palazzi,
503 E., Rangwala, I., Schöner, W., Severskiy, I., Shahgedanova, M., Wang, M. B.,
504 Williamson, S. N., Yang, D. Q., and Mountain Research Initiative, E. D. W. W. G.:
505 Elevation-dependent warming in mountain regions of the world, *Nature Climate Change*,
506 5, 424-430, 10.1038/nclimate2563, 2015.

507 Pierce, D. W., Das, T., Cayan, D. R., Maurer, E. P., Miller, N. L., Bao, Y., Kanamitsu, M.,
508 Yoshimura, K., Snyder, M. A., and Sloan, L. C.: Probabilistic estimates of future changes
509 in California temperature and precipitation using statistical and dynamical downscaling,
510 *Climate Dynamics*, 40, 839-856, 2013.

511 Qiu, Y., Hu, Q., and Zhang, C.: WRF simulation and downscaling of local climate in Central
512 Asia, *International Journal of Climatology*, 37, 513-528, 10.1002/joc.5018, 2017.

513 Qiu, Y., Feng, J., Yan, Z., Wang, J., and Li, Z.: High-resolution dynamical downscaling for
514 regional climate projection in Central Asia based on bias-corrected multiple GCMs,
515 *Climate Dynamics*, 10.1007/s00382-021-05934-2, 2021.

516 Racherla, P., Shindell, D., and Faluvegi, G.: The added value to global model projections of
517 climate change by dynamical downscaling: A case study over the continental US using
518 the GISS-ModelE2 and WRF models, *Journal of Geophysical Research: Atmospheres*,
519 117, 2012.

520 Rangwala, I., Sinsky, E., and Miller, J. R.: Amplified warming projections for high altitude
521 regions of the northern hemisphere mid-latitudes from CMIP5 models, *Environmental*
522 *Research Letters*, 8, 024040, 10.1088/1748-9326/8/2/024040, 2013.

523 Seddon, A. W., Macias-Fauria, M., Long, P. R., Benz, D., and Willis, K. J.: Sensitivity of
524 global terrestrial ecosystems to climate variability, *Nature*, 531, 229-232, 2016.

525 Skamarock, W. C., Klemp, J. B., Dudhia, J., Gill, D. O., Barker, D. M., Wang, W., and Powers,
526 J. G.: A description of the Advanced Research WRF version 3. NCAR Technical note-
527 475+ STR, 2008.

528 Sorg, A., Bolch, T., Stoffel, M., Solomina, O., and Beniston, M.: Climate change impacts on
529 glaciers and runoff in Tien Shan (Central Asia), *Nature Climate Change*, 2, 725-731,
530 10.1038/nclimate1592, 2012.

531 Tang, J., Niu, X., Wang, S., Gao, H., Wang, X., and Wu, J.: Statistical downscaling and
532 dynamical downscaling of regional climate in China: Present climate evaluations and
533 future climate projections, *Journal of Geophysical Research: Atmospheres*, 121, 2110-
534 2129, <https://doi.org/10.1002/2015JD023977>, 2016.

535 Thurman, M.: Natural disaster risks in Central Asia: a synthesis, UNDP/BCPR, Regional
536 Disaster Risk Reduction Asvisor, Europe and CIS, 2011.

537 Torma, C., Giorgi, F., and Coppola, E.: Added value of regional climate modeling over areas
538 characterized by complex terrain—Precipitation over the Alps, *Journal of Geophysical*
539 *Research: Atmospheres*, 120, 3957-3972, 10.1002/2014JD022781, 2015.

540 Vautard, R., Gobiet, A., Jacob, D., Belda, M., Colette, A., Déqué, M., Fernández, J., García-
541 Díez, M., Goergen, K., Gütler, I., Halenka, T., Karacostas, T., Katragkou, E., Keuler, K.,
542 Kotlarski, S., Mayer, S., van Meijgaard, E., Nikulin, G., Patarčić, M., Scinocca, J.,
543 Sobolowski, S., Suklitsch, M., Teichmann, C., Warrach-Sagi, K., Wulfmeyer, V., and
544 Yiou, P.: The simulation of European heat waves from an ensemble of regional climate
545 models within the EURO-CORDEX project, *Climate Dynamics*, 41, 2555-2575,

546 10.1007/s00382-013-1714-z, 2013.

547 Wang, J., and Kotamarthi, V. R.: High-resolution dynamically downscaled projections of
548 precipitation in the mid and late 21st century over North America, *Earth's Future*, 3, 268-
549 288, 2015.

550 Wang, W., Barker, D., Bray, J., Bruyere, C., Duda, M., Dudhia, J., Gill, D., Michalakes, J. J.
551 M., and Research, M. M. D. N. C. f. A.: User's guide for advanced research WRF (ARW)
552 modeling system version 3, 2007.

553 Wang, X., Huang, G., Liu, J., Li, Z., and Zhao, S.: Ensemble projections of regional climatic
554 changes over Ontario, Canada, *Journal of Climate*, 28, 7327-7346, 2015.

555 Wang, Y., Feng, J., Luo, M., Wang, J., and Qiu, Y.: Uncertainties in simulating central Asia:
556 Sensitivity to physical parameterizations using Weather Research and Forecasting model,
557 *International Journal of Climatology*, 40, 5813-5828, <https://doi.org/10.1002/joc.6567>,
558 2020.

559 Xu, Z., and Yang, Z.-L.: An Improved Dynamical Downscaling Method with GCM Bias
560 Corrections and Its Validation with 30 Years of Climate Simulations, *Journal of Climate*,
561 25, 6271-6286, 10.1175/JCLI-D-12-00005.1, 2012.

562 Zhang, C., Lu, D., Chen, X., Zhang, Y., Maisupova, B., and Tao, Y.: The spatiotemporal
563 patterns of vegetation coverage and biomass of the temperate deserts in Central Asia and
564 their relationships with climate controls, *Remote Sens Environ*, 175, 271-281,
565 10.1016/j.rse.2016.01.002, 2016.

566 Zhu, X., Wei, Z., Dong, W., Ji, Z., Wen, X., Zheng, Z., Yan, D., and Chen, D.: Dynamical
567 downscaling simulation and projection for mean and extreme temperature and
568 precipitation over central Asia, *Climate Dynamics*, 10.1007/s00382-020-05170-0, 2020.

569 Zittis, G., Hadjinicolaou, P., Klangidou, M., Proestos, Y., and Lelieveld, J.: A multi-model,
570 multi-scenario, and multi-domain analysis of regional climate projections for the
571 Mediterranean, *Regional Environmental Change*, 19, 2621-2635, 10.1007/s10113-019-
572 01565-w, 2019.

573 Zou, L., and Zhou, T.: Future summer precipitation changes over CORDEX-East Asia domain
574 downscaled by a regional ocean-atmosphere coupled model: A comparison to the stand-
575 alone RCM, *Journal of Geophysical Research: Atmospheres*, 121, 2691-2704,
576 <https://doi.org/10.1002/2015JD024519>, 2016.

577 Zou, L., and Zhou, T.: Dynamical downscaling of East Asian winter monsoon changes with a
578 regional ocean-atmosphere coupled model, *Quarterly Journal of the Royal
579 Meteorological Society*, 143, 2245-2259, <https://doi.org/10.1002/qj.3082>, 2017.

580

581 **Tables**

582 **Table 1** Geostatic variables and meteorological elements in the HCPD-CA dataset

Name	Description	Unit
HGT	Terrain height	m
LU_INDEX	Land use category	-
LANDMASK	Land mask (1 for land, 0 for water)	-
ISLTYP	Soil category	-

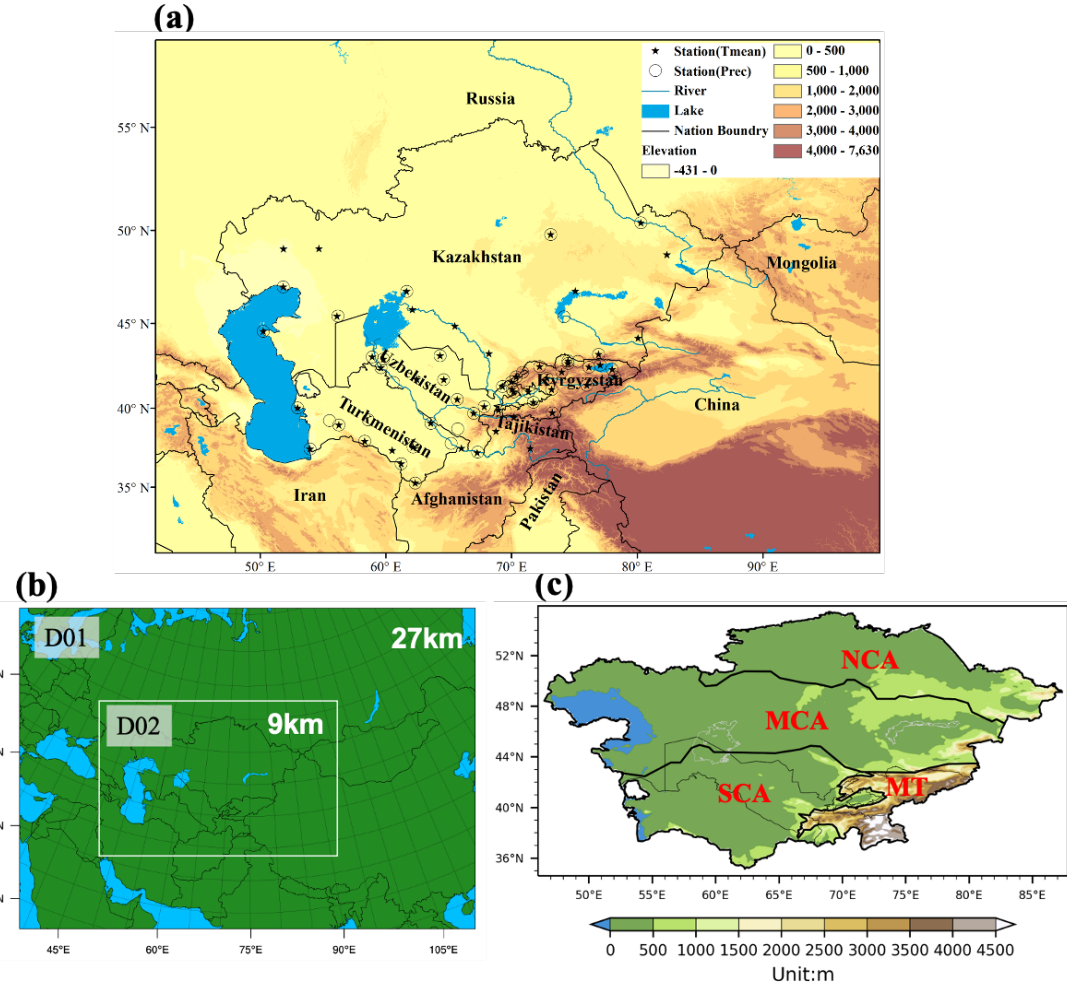
PREC	Daily precipitation	mm/day
T2MEAN	Daily mean temperature at 2m	K
T2MAX	Daily maximum temperature at 2m	K
T2MIN	Daily minimum temperature at 2m	K
RH2MEAN	Daily mean relative humidity at 2m	%
U10MEAN	Daily mean eastward wind at 10m	m/s
V10MEAN	Daily mean northward wind at 10m	m/s
SWD	Daily mean downwelling shortwave flux at bottom	W/m ²
LWD	Daily mean downwelling longwave flux at bottom	W/m ²
PSFC	Daily mean surface pressure	Pa

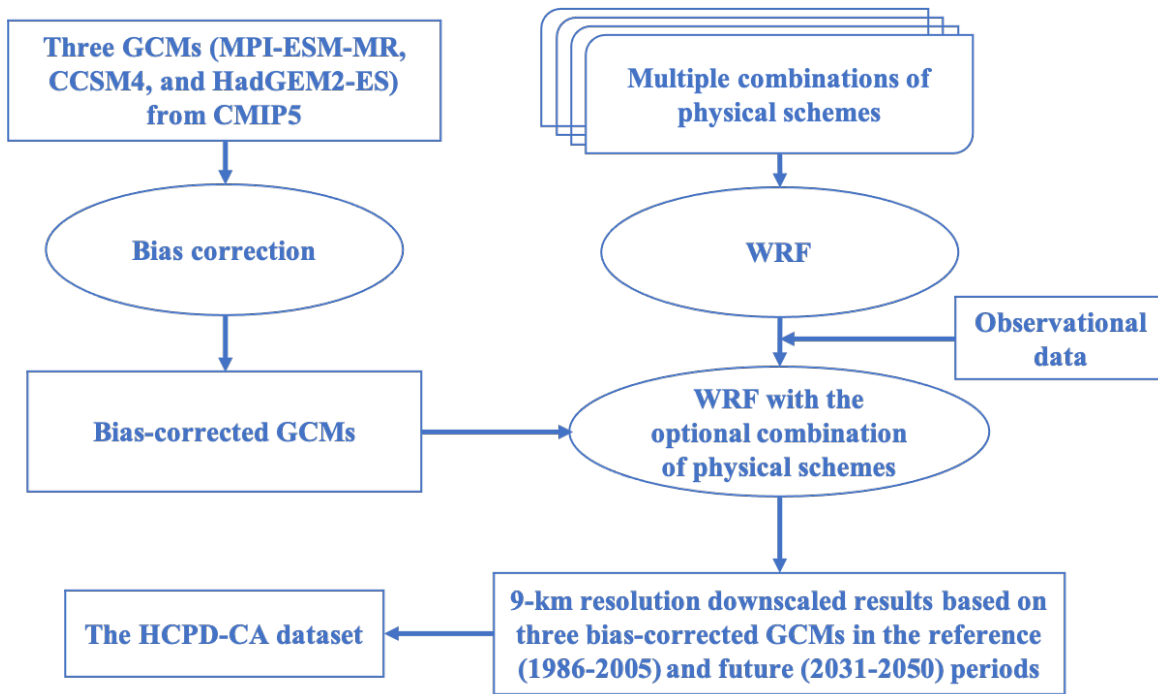
583
584
585
586
587

Table 2 Information about the datasets used in the study.

Dataset	Run	Spatial	Temporal	Link
		Resolution	Resolution	
MPI-ESM-MR	r1i1p1	$1.9^\circ \times 1.9^\circ$	6-hourly	https://esgf-node.llnl.gov/projects/cmip5/
HadGEM2-ES	r1i1p1	$1.3^\circ \times 1.9^\circ$	6-hourly	https://esgf-node.llnl.gov/projects/cmip5/
CCSM4	b40.[20th\RCP 4.5].track1.1de g.012.cam2.h4	$0.9^\circ \times 1.3^\circ$	6-hourly	https://rda.ucar.edu/datasets/ds316.0/#/access
ERA-Interim	-	$0.75^\circ \times 0.75^\circ$	Synoptic monthly means	https://apps.ecmwf.int/datasets/data/interim-full-mnths/levtype=sfc/
CRU TS v4	-	$0.5^\circ \times 0.5^\circ$	monthly	https://crudata.uea.ac.uk/cru/data/hrg/cru_ts_4.00/
ERA5-Land	-	$0.1^\circ \times 0.1^\circ$	monthly	https://cds.climate.copernicus.eu/cdsapp#!/dataset/reanalysis-era5-land-monthly-means?tab=form

599 **Figures**

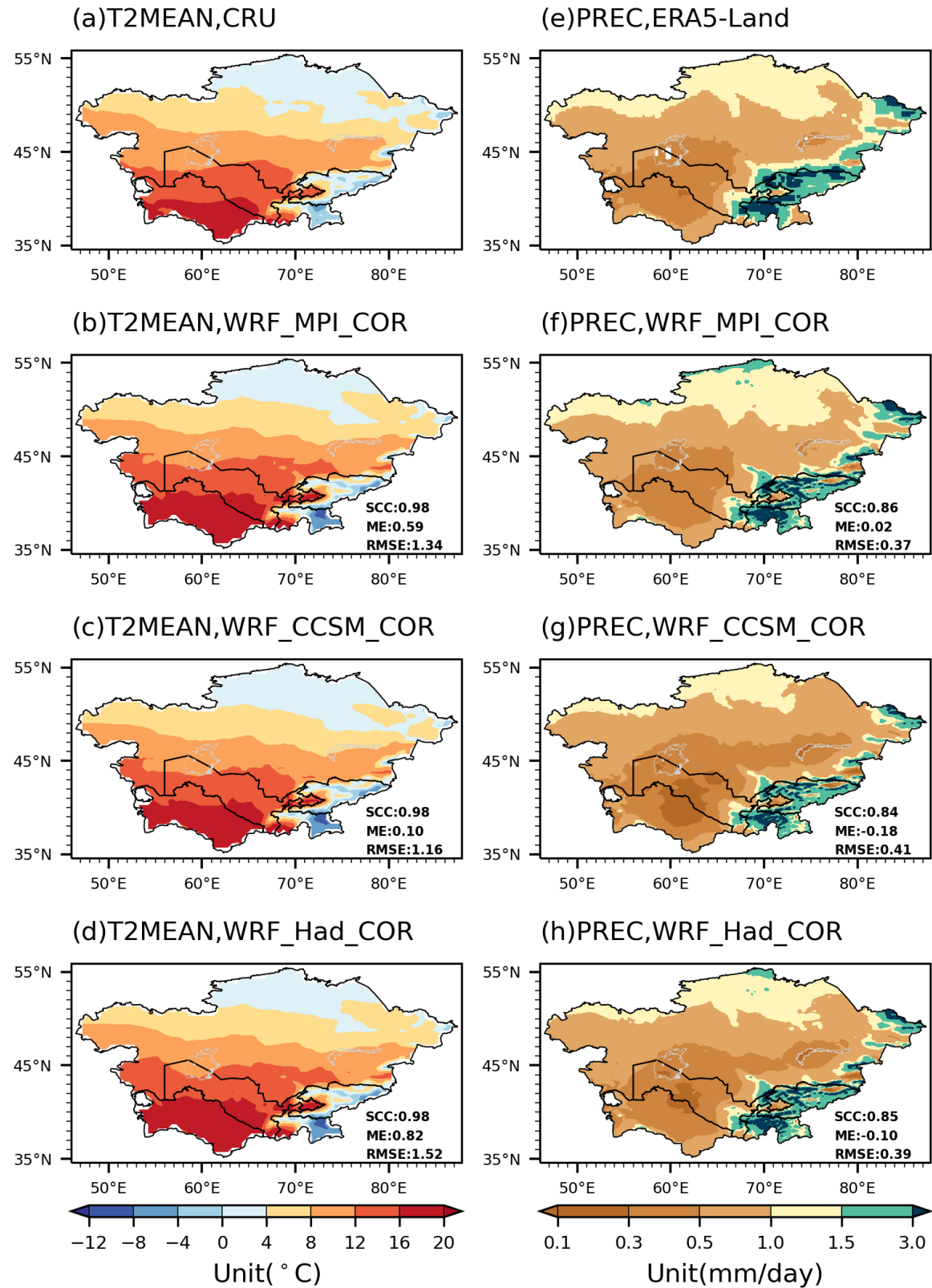




607

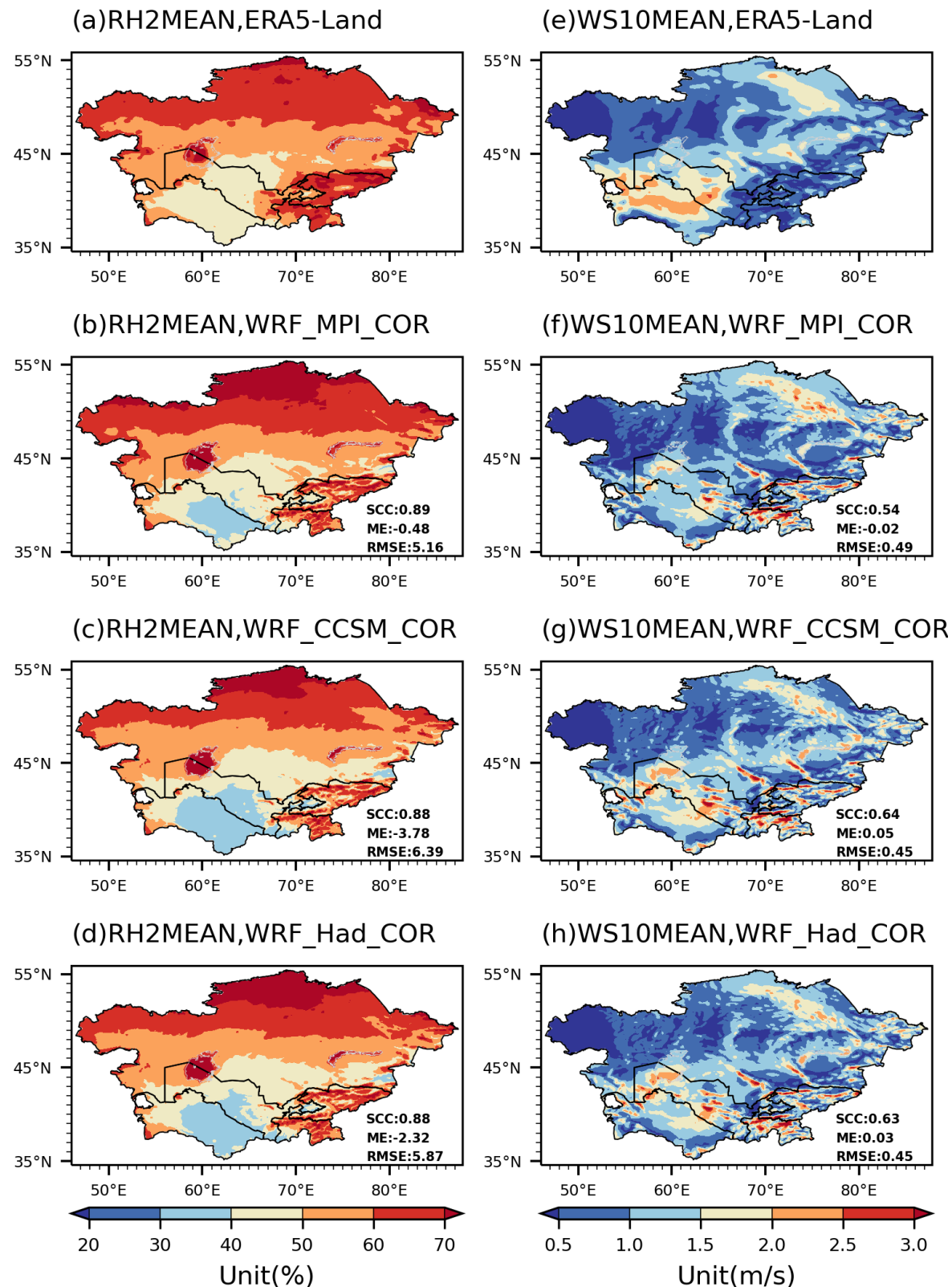
608

Fig. 2 Flow chart for the HCPD-CA dataset.



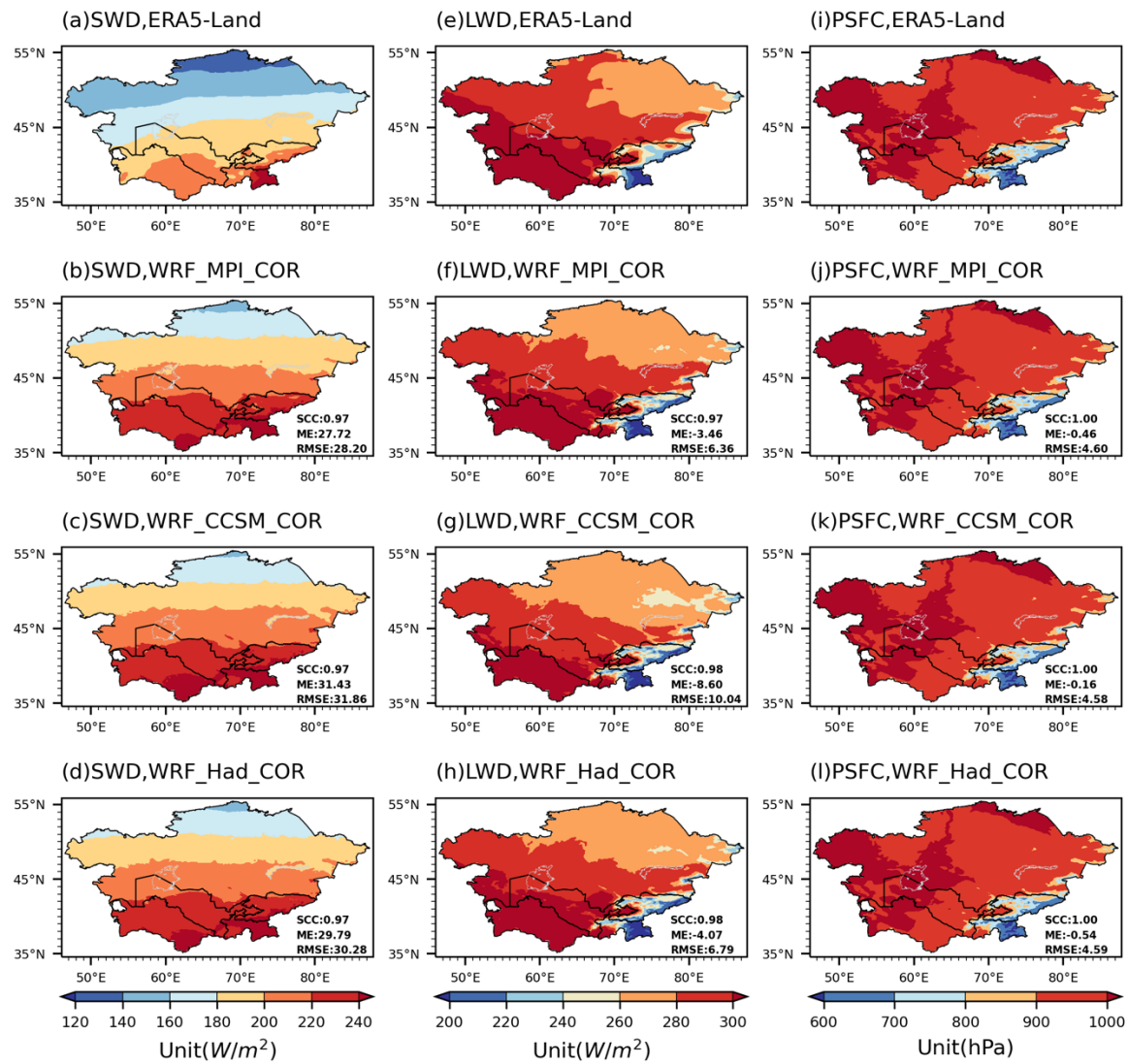
609

610 **Fig. 3** The observed and simulated annual mean T2MEAN and PREC in Central Asia during
 611 the reference period (1986-2005). The spatial correlation coefficient (SCC), mean error (ME),
 612 and root mean square error (RMSE) are listed.



613

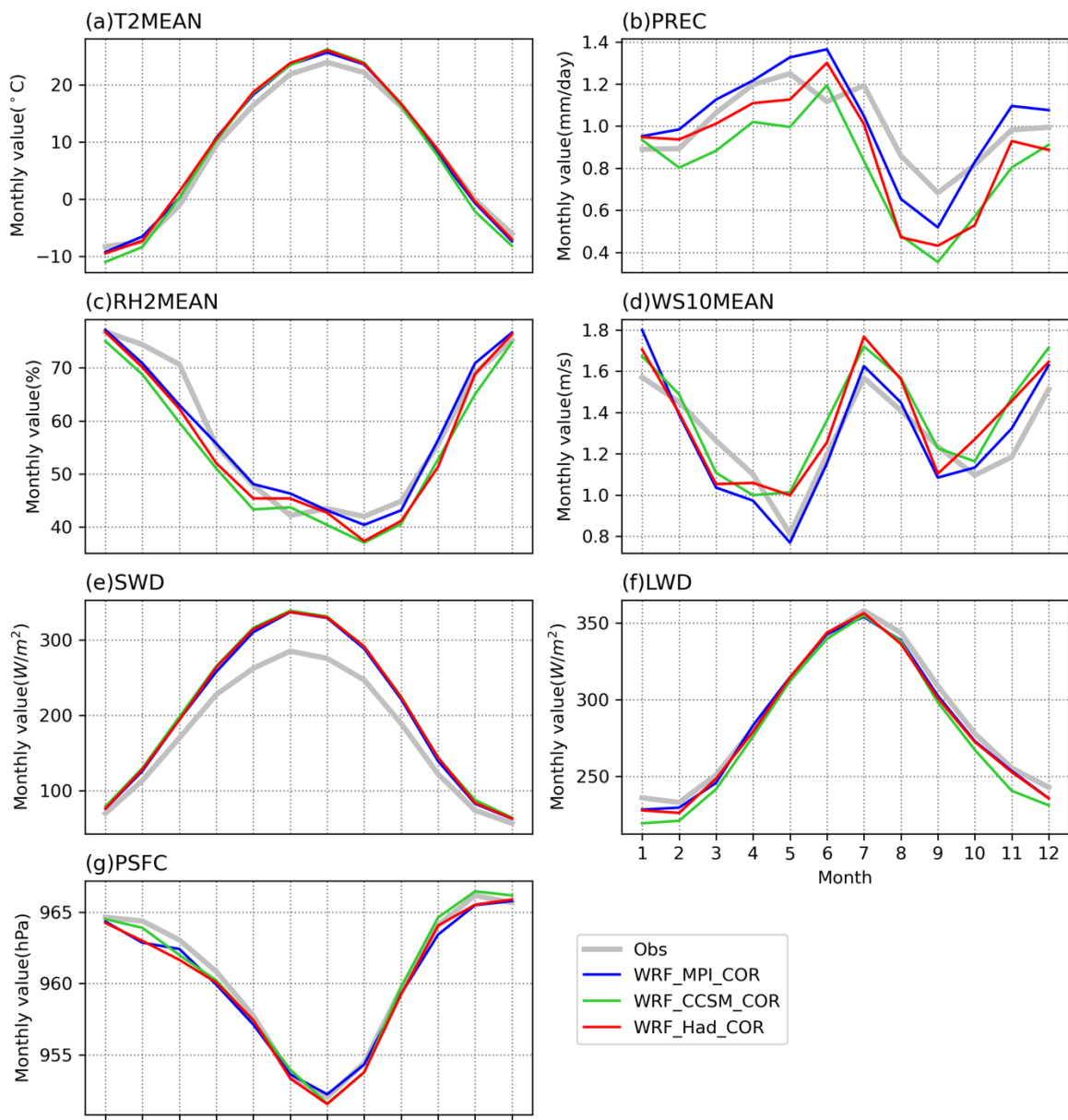
614 **Fig. 4** Same as **Fig. 3**, but for annual mean RH2MEAN and WS10MEAN.



615

616 **Fig. 5** Same as **Fig. 3**, but for annual mean SWD, LWD, and PSFC.

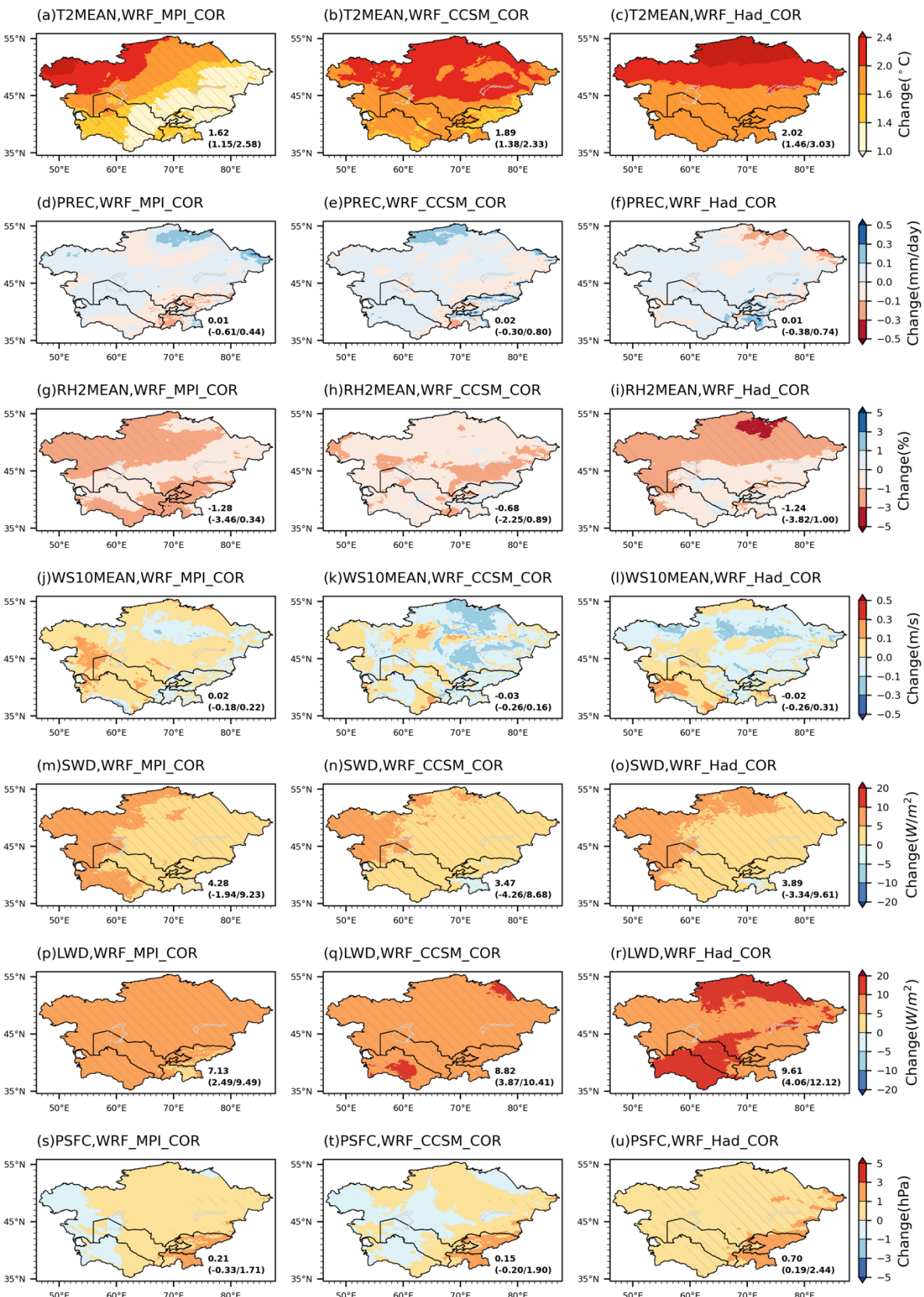
617



618

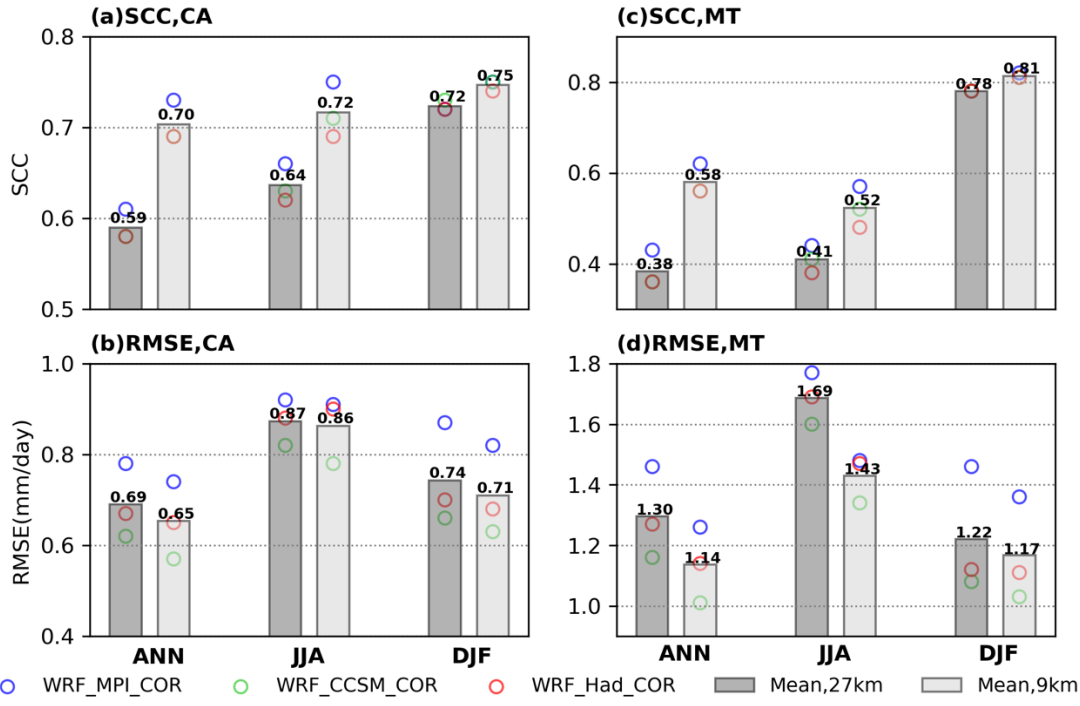
619 **Fig. 6** Mean annual cycle of the monthly values averaged over Central Asia in the
620 observations and RCM simulations.

621



622

623 **Fig. 7** Projected changes of the annual mean values over Central Asia during 2031-2050,
 624 relative to 1986-2005. The regional mean (upper), minimum and maximum value (in
 625 parentheses) are listed. The slashed areas indicate where the changes passed the significance
 626 test at the 95% confidence level using the two-tailed Student's t test.



629 **Fig. 8** Spatial correlation coefficients (SCCs) and root mean square errors (RMSEs) of the
630 simulated annual (ANN), summer (JJA: June-July-August), and winter (DJF: December-
631 January-February) mean precipitation over CA and the mountainous areas (MT) in the 9-km
632 and 27-km resolution downscaled results. The metrics are calculated based on 52 stations'
633 data across CA.